Geophysical Research Letters

RESEARCH LETTER
10.1029/2019GL082914

Radiative Heating of an Ice-Free Arctic Ocean

Kristina Pistone[1], **Ian Eisenman**[2], **and Veerabhadran Ramanathan**[2]

[1]Bay Area Environmental Research Institute, NASA Ames Research Center, Moffett Field, CA, USA, [2]Scripps Institution of Oceanography, University of California San Diego, La Jolla, CA, USA

Key Points:
- The complete disappearance of Arctic sea ice would contribute an additional solar radiative heating of 0.71 W/m^2 to the planet
- This is equivalent to the radiative forcing from one trillion tons of CO_2 emissions
- The added solar heating from complete Arctic sea ice loss would be an order of magnitude larger in the month of May than in the month of September

Supporting Information:
- Supporting Information S1

Correspondence to:
K. Pistone,
kristina.pistone@fulbrightmail.org

Citation:
Pistone, K., Eisenman, I., & Ramanathan, V. (2019). Radiative heating of an ice-free arctic ocean. *Geophysical Research Letters*, *46*, 7474–7480. https://doi.org/10.1029/2019GL082914

Received 21 MAR 2019
Accepted 15 JUN 2019
Accepted article online 20 JUN 2019
Published online 10 JUL 2019

Abstract During recent decades, there has been dramatic Arctic sea ice retreat. This has reduced the top-of-atmosphere albedo, adding more solar energy to the climate system. There is substantial uncertainty regarding how much ice retreat and associated solar heating will occur in the future. This is relevant to future climate projections, including the timescale for reaching global warming stabilization targets. Here we use satellite observations to estimate the amount of solar energy that would be added in the worst-case scenario of a complete disappearance of Arctic sea ice throughout the sunlit part of the year. Assuming constant cloudiness, we calculate a global radiative heating of 0.71 W/m^2 relative to the 1979 baseline state. This is equivalent to the effect of one trillion tons of CO_2 emissions. These results suggest that the additional heating due to complete Arctic sea ice loss would hasten global warming by an estimated 25 years.

1. Introduction

Much recent work has investigated the conditions under which global warming is limited to 2 or 1.5°C, which are the targets included in the Paris Climate Accord. Recent analyses suggest that these targets are becoming increasingly difficult to achieve (Millar et al., 2017). With continuing unchecked emissions of climate warming pollutants, global warming is projected to have a 50% probability of exceeding the 2°C threshold by 2050 (Xu & Ramanathan, 2017).

Climate models suggest a wide range of levels of sea ice retreat associated with 2°C of global warming, including the possibility that the Arctic Ocean becomes ice free at the end of each summer (Jahn, 2018; Screen & Williamson, 2017; Sigmond et al., 2018) yet with some ice still remaining in the midsummer season when solar insolation peaks. The disappearance of sea ice alters the Earth's energy balance because a low-albedo open ocean surface typically absorbs approximately 6 times more solar radiation than a surface covered with sea ice and snow, which has a substantially higher albedo (e.g., Perovich, 1998). This can play a substantial role in the energy balance of the climate system. Satellite observations suggest that the albedo changes associated with the decline of Arctic sea ice during 1979–2011 contributed a global-mean increase in solar heating of 0.21 W/m^2, which is a quarter as large as the direct radiative forcing from rising CO_2 concentrations during the same period (Pistone et al., 2014).

In this study we consider the additional solar heating associated with the extreme worst-case scenario in which a complete disappearance of Arctic sea ice throughout the sunlit part of the year occurs far earlier than in climate model projections.

2. Climate Model Projections of Arctic Sea Ice Loss

Comprehensive global climate models differ widely in terms of the level of global warming at which the Arctic becomes ice free. Results from the suite of climate models included in the Coupled Model Intercomparison Project Phase 5 (CMIP5) are shown in Figure 1. Although these simulations do not typically reach annually ice-free conditions, the level of global warming at which the simulated Arctic Ocean would be annually ice free can be estimated from the simulations. Previous studies have shown that the annual-mean Arctic sea ice area follows an approximately linear relationship with global-mean temperature (Gregory et al., 2002; Rosenblum & Eisenman, 2017; Winton, 2011) and similarly with cumulative carbon dioxide emissions (Notz & Stroeve, 2016). The sea ice sensitivity to global warming remains fairly constant in each model as the simulated climate changes. Based on the sea ice cover in the 1979 baseline state (Figure 1a)

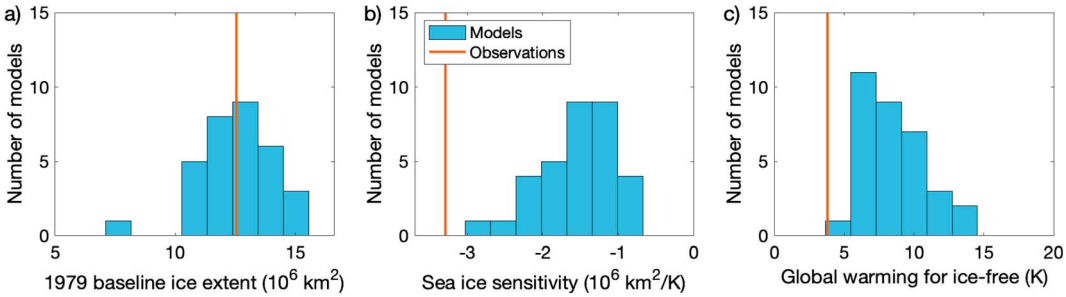

Figure 1. Annual-mean Arctic sea ice cover and global-mean temperature in Coupled Model Intercomparison Project Phase 5 climate model simulations. (a) The 1979 baseline sea ice extent (see Appendix A). (b) The change in sea ice extent per change in global-mean temperature (i.e., the sea ice sensitivity). (c) Estimate of the level of global warming relative to 1979 at which the Arctic Ocean becomes completely ice free, which is the ratio of the value in panel (a) to the value in panel (b). The processed model output is adopted from Rosenblum and Eisenman (2017). The solid red line in each panel shows ice extent and global-mean temperature values from the observational record. Details are given in Appendix A.

and the sea ice sensitivity to global warming (Figure 1b) in each simulation (see Appendix A below), we find that the CMIP5 ensemble-mean result implies that the Arctic Ocean would be annually ice free under 8.7°C of global warming (Figure 1c). There is a relatively wide spread among the model simulations in Figure 1c, which may be due in part to factors related to internal climate variability (Kay et al., 2011; Rosenblum & Eisenman, 2017) in addition to differences in model physics. However, there is a striking bias between the modeled Arctic sea ice changes and the observations. The observed Arctic sea ice retreat per degree of global warming is 2.1 times larger than the CMIP5 ensemble-mean result, with no model (blue histogram in Figure 1b) simulating a value as extreme as the observations (red line in Figure 1b). This suggests that there may be substantial systematic biases in the model projections of the level of global warming at which the Arctic becomes annually ice free. Given that this bias exists in the models and that future changes may not follow past observations due to internal climate variability and other factors, we cannot exclude the extreme possibility that the Arctic could become annually ice free during the coming decades. This extreme possibility is the focus of the current study.

3. Radiative Heating of an Ice-Free Arctic Ocean Based on Satellite Observations

In order to bypass issues associated with these model biases, we use direct satellite observations to assess the impact of an annually ice-free Arctic Ocean. We examine the planetary (i.e., top of atmosphere) albedo during the 17-year Clouds and the Earth's Radiant Energy System (CERES) record above ice-free locations in the Arctic Ocean. This provides an estimate of the planetary albedo associated with an ice-free ocean surface in a range of latitudes, seasons, and cloud conditions, which, together with an estimate for future cloud conditions, allows us to estimate the additional solar heating that would occur under the complete disappearance of Arctic sea ice during the sunlit part of the year (see discussion of data, methodology, and assessment of cloud conditions in Appendix A and Text S2 of the supporting information). Hence, the approach adopted here essentially relies on spatial interpolation of observed conditions. This is in contrast to an extrapolation of the observed relationship between changes in the top-of-atmosphere albedo of the Arctic region (Pistone et al., 2014) and changes in Arctic sea ice. The latter approach approximately holds over relatively small changes in ice extent and albedo, but it is not expected to provide an accurate estimate under the substantial extrapolation to 100% ice loss from the observed 18% loss of annual-mean ice extent during 1979–2016 (Fetterer et al., 2017; based on the endpoints of a linear fit as a fraction of the 1979-2016 mean).

A source of uncertainty in the present analysis is how cloudiness above the Arctic Ocean may change in the future in response to sea ice retreat. Previous findings suggest that the fractional cloud cover and average cloud optical properties may remain approximately unchanged, which we adopt here as a baseline estimate. Specifically, previous work found the relationship between planetary albedo and Arctic sea ice cover during 2000–2011 to be consistent with a time-invariant cloud albedo field (Pistone et al., 2014), despite substantial sea ice retreat occurring during this period. Another recent study found an increase in Arctic cloud fraction

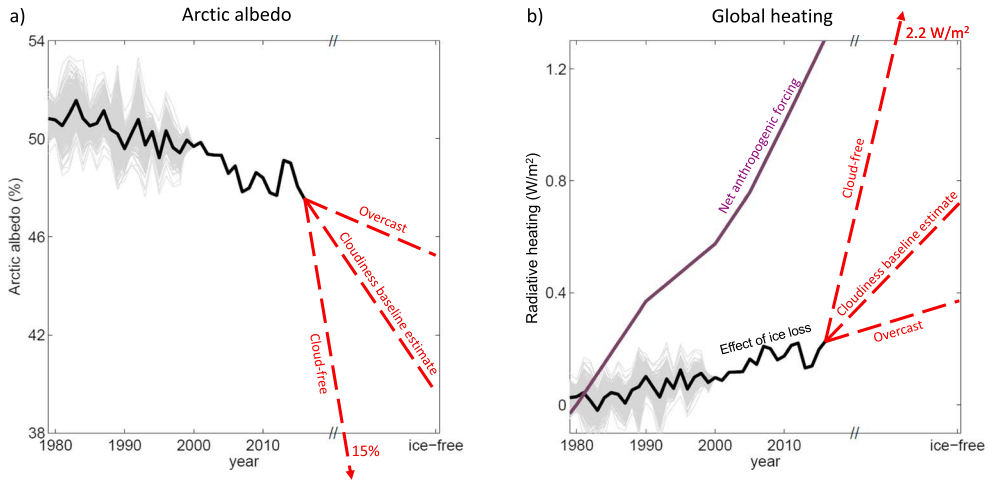

Figure 2. Albedo and radiative heating from observed Arctic sea ice retreat and projections of ice-free Arctic Ocean conditions. Annually averaged (a) Arctic albedo and (b) global-mean increase in all-sky absorbed solar energy relative to 1979 for the observational period (1979–2016, black line) and the three cloud scenarios considered in the text (red dashed lines). The observational values are from the Clouds and the Earth's Radiant Energy System (CERES) measurements during 2000–2016 and CERES-based historical estimates (Pistone et al., 2014) for 1979–1999. The cloud scenarios include a baseline estimate that holds the cloud fraction and optical depth distributions as in present-day observations, completely overcast conditions above the Arctic Ocean with the cloud optical depth distribution as in present-day observations, and a completely cloud-free Arctic Ocean. Ice-free conditions for the latter cloud-free case are outside the plotted ranges: for this case, the Arctic albedo is 15% and the change in radiative heating is 2.24 W/m^2. The gray thin lines show an estimate of the envelope of uncertainty for the historical estimates (see Appendix A). The purple solid line in panel (b) indicates an estimate of total radiative heating (RCP Database, 2009).

in the fall and spring but no discernible change in cloud fraction or cloud optical depth associated with sea ice changes in summertime (Morrison et al., 2018), which is the season with greatest insolation. This finding is also consistent with earlier work (Kay & Gettelman, 2009).

Hence, we focus on the baseline estimate scenario in which cloud conditions remain unchanged from the present. We find that the complete disappearance of Arctic sea ice throughout the sunlit part of the year in this scenario would cause the average planetary albedo of the Arctic Ocean (poleward of 60°N) to decrease by 11.5% in absolute terms. This would add an additional 21 W/m^2 of annual-mean solar heating over the Arctic Ocean relative to the 1979 baseline state. Averaged over the globe, this implies a global radiative heating of 0.71 W/m^2 (Figure 2).

Several previous studies have also included estimates of the solar heating associated with the Arctic becoming completely ice-free using approaches that differ from the present study. One study estimated the global-mean radiative effect associated with the presence of the Arctic sea ice using modeled radiative kernels and a range of model-based and satellite-based surface albedos, and they found it to be −0.65 W/m^2 (Flanner et al., 2011). Another study used an albedo product from the satellite-borne Advanced Very-High-Resolution Radiometer instrument combined with a kernel method to estimate this value to be −0.825 W/m^2 (Cao et al., 2015). Lastly, a study used CERES albedo observations through 2011, assuming that the seasonal cycle in cloud fraction does not change and specifying each season and location as either dark ice, bright ice, or ice-free ocean, and estimated that completely ice-free conditions would cause 0.68 W/m^2 of radiative heating (Hudson, 2011). These values are fairly similar to the estimate in the present study of 0.71 W/m^2, despite the previous studies using markedly different approaches.

4. Discussion

Of the 0.71 W/m^2 of globally averaged heating, 0.21 W/m^2 is estimated to have already occurred between 1979 and 2016. Approximately half (0.11 W/m^2) of this realized heating occurred during the CERES observational record (2000–2016), with the other half occurring between 1979 and 1999 as estimated based on the observed relationship between satellite-derived sea ice concentration and albedo (Pistone et al., 2014).

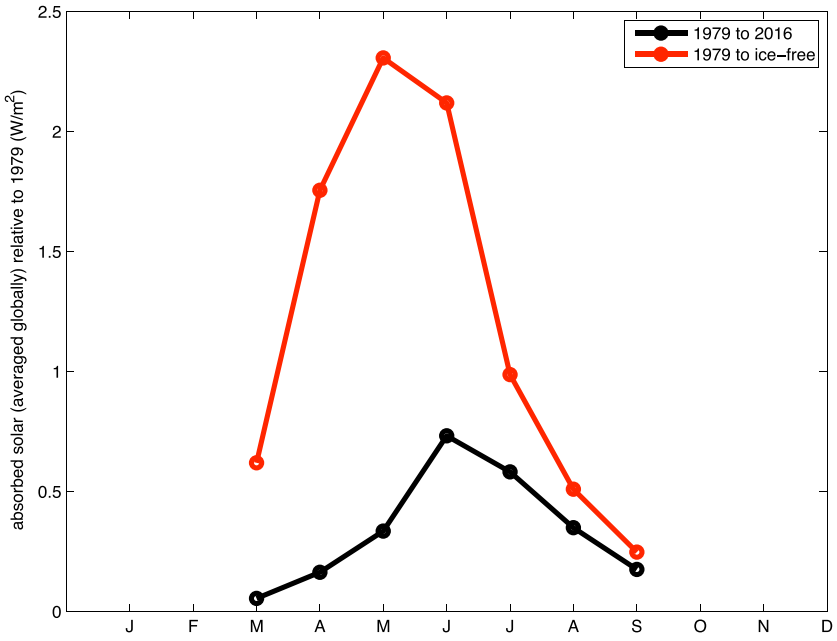

Figure 3. Seasonal structure of the change in absorbed solar radiation. Globally averaged values are plotted for the radiative heating associated with sea ice loss during 1979–2016 (black line) and under the complete loss of Arctic sea ice relative to 1979 using the baseline estimate of invariant cloudiness conditions (red line). Note that the annual-mean values of the black and red curves are 0.21 and 0.71 W/m^2, respectively, as described in the main text, and are calculated assuming zero solar forcing during the winter months (October–February).

This heating of 0.71 W/m^2 is approximately equivalent to the direct radiative effect of emitting one trillion tons of CO_2 into the atmosphere (see calculation in Appendix A). As of 2016, an estimated 2.4 trillion tons of CO_2 have been emitted since the preindustrial period due to both fossil fuel combustion (1.54 trillion tons) and land use changes (0.82 trillion tons), with an additional 40 billion tons of CO_2 per year emitted from these sources during 2007–2016 (Le Quéré et al., 2018). Thus, the additional warming due to the complete loss of Arctic sea ice would be equivalent to 25 years of global CO_2 emissions at the current rate. This implies that if the Arctic sea ice were to disappear much more rapidly than in current climate model projections, it would drastically shorten the time available to adapt to climate changes and the time for achieving carbon neutrality.

Next, we consider the uncertainty in this analysis due to possible cloudiness changes during the loss of the sea ice. We examine two perhaps unrealistically extreme future Arctic cloud scenarios: at one extreme, an ice-free Arctic Ocean that is completely cloud free and at the other extreme, an ice-free Arctic Ocean that is completely overcast. For simplicity, in the latter scenario we use distributions of cloud optical thickness based on present-day observations (see Appendix A). Both of these extreme scenarios are shown in Figure 2. The cloud-free, ice-free Arctic scenario results in a global radiative heating of 2.2 W/m^2 compared with the 1979 baseline state, which is 3 times more than the 0.71 W/m^2 baseline estimate derived above for unchanged clouds. The completely overcast ice-free Arctic scenario results in a global radiative heating of 0.37 W/m^2, which is approximately half as large as the 0.71 W/m^2 baseline estimate (Figure 2b). This suggests that even in the presence of an extreme negative cloud feedback, the global heating due to the complete disappearance of the Arctic sea ice would still be nearly double the already-observed heating due to the current level of ice loss.

Note that the ice albedo climate feedback describes how (i) there is ice loss associated with global warming and (ii) this ice loss leads to radiative heating. Hence, this feedback is typically expressed in terms of the amount of additional heating per degree of global warming. The present study focuses on the additional radiative heating from the complete loss of Arctic sea ice, but it does not estimate the amount of global warming that would be associated with this level of ice loss.

Much previous attention has been focused on sea ice during the month of September, which is the time of summer minimum ice extent and also the month that has seen the fastest rate of ice extent retreat in recent

decades. We examine the seasonal structure of the radiative heating due to sea ice changes in Figure 3, which shows the contributions from each month to the total global heating for the observed ice loss between 1979 and 2016 (black curve) and for the complete loss of Arctic sea ice (red curve). For both curves, the greatest heating occurs several months before September. The occurrence of the insolation maximum in midsummer, as well as other factors such as the seasonal cycle of cloud conditions (Figures S3–S5 of the supporting information), causes the radiative heating from the observed sea ice loss (Figure 3, black curve) to peak in June, despite the observed ice extent loss being substantially smaller during June than during September (e.g., Figure S1 of Pistone et al., 2014). The radiative heating associated with a complete loss of sea ice peaks in May (Figure 3, red curve). This shift to 1 month earlier is likely associated with there being more sea ice to lose relative to the 1979 baseline state in May than in June, in contrast to the observed sea ice extent retreat being faster in June than in May (e.g., Figure 1 of Eisenman, 2010). However, the similarity between the two curves in Figure 3 suggests that even under conditions in which the Arctic Ocean becomes ice free only in September, the additional radiative heating may likely be driven largely by the associated midsummer sea ice loss.

5. Conclusions

In summary, the results presented here suggest a potentially substantial contribution to the radiative heating of the global climate due to the loss of Arctic sea ice. We find that the extreme case of a complete disappearance of the Arctic sea ice cover throughout the sunlit months would cause an annual-mean global-mean radiative heating of 0.71 W/m^2. This is equivalent to one trillion tons of additional CO_2 emissions. An important caveat is that there is substantial uncertainty in the timing of future Arctic sea ice retreat, and it is possible that such an extreme loss will not occur in the coming century. Nonetheless, these results imply that the radiative heating due to this worst-case scenario of complete Arctic sea ice loss could substantially accelerate the rate of future global warming, advancing global warming by 25 years.

Appendix A: Data and Methods

In the calculations of albedo and radiative heating presented here, we use data from the National Aeronautics and Space Administration's CERES Terra SSF Edition 4 monthly averaged 1 × 1-degree product, between March 2000 and October 2016, available online (https://ceres.larc.nasa.gov/order_data.php). The Arctic Ocean is defined here as the land-free area poleward of 60°N. Due to issues concerning polar night, we only consider the months of March to September of each year. As in Pistone et al. (2014, hereafter PER2014), here we consider changes in only the shortwave component of the total energy balance. The analysis of CERES shortwave data (Wielicki et al., 1996) and satellite sea ice concentration data (Comiso, 2017) used to generate the 1979–2016 values plotted in Figure 2 follows the methodology described in PER2014: we use the observed relationship between albedo and sea ice concentration in each season and region of the Arctic during the CERES period (2000–2016) in order to reconstruct albedo during the earlier period when only sea ice concentration observations are available (1979–2000). This analysis was updated from PER2014 in the present study to include the longer period of observations and the newer Edition of CERES data currently available; these updates are summarized in Text S1 of the supporting information.

Our estimate of an ice-free future Arctic Ocean analyzes observed ice-free locations in the Arctic Ocean, which are defined here as locations where the value of the snow/ice percent field included with the CERES data product is zero. We draw on separate but analogous calculations for clear-sky and overcast conditions. For clear-sky conditions, we rely on the observed approximately linear relationship between (i) the clear-sky albedo reported in the CERES data for each grid box above ice-free ocean regions and (ii) the cosine of solar zenith angle (which is determined by latitude and season; see Figure S1 of the supporting information). We use this relationship to estimate the clear-sky albedo associated with ice-free conditions over all Arctic Ocean latitudes and seasons, including those that have always been ice covered during the satellite record. This estimate is used for the scenario in which the Arctic becomes cloud free when the sea ice is lost. For completely overcast conditions (defined here as grid boxes with cloud fraction greater than 95%), we find that the observed albedo above ice-free ocean regions exhibits a similar relationship and also depends on the cloud optical depth (Figure S2 of the supporting information), thus allowing estimation of the ice-free albedo for a uniform cloud population (as defined by optical depth). We approximate that the frequency distributions of cloud optical depth over the Arctic Ocean will remain invariant during sea ice retreat (see

discussion in Text S2 of the supporting information). This estimate is used for the scenario in which the Arctic becomes completely overcast when the sea ice is lost. Next, we take a weighted mean of these two scenarios based on the observed distribution of cloud fraction, and we use this to calculate the baseline estimate scenario in which the cloud cover remains unchanged when the sea ice is lost. In other words, the baseline estimate scenario assumes that the future distributions of cloud fraction and cloud optical depth over the Arctic Ocean will be approximately unchanged from present-day conditions (2000–2016 mean) when the sea ice is lost. Further details are given in the Text S2 of the supporting information, which draws on a number of other previous studies (Bender et al., 2011; Engstrom et al., 2015; Bender et al., 2017).

In order to minimize the effects of variability in single years, we compute changes during 1979–2016 from the endpoints of an ordinary least squares linear fit to the 1979–2016 yearly data. The 1979 baseline state which is compared with ice-free conditions is similarly defined as the 1979 value of this 1979–2016 linear fit. This is done for each month of the year in Figure 3, and the annual average of these values (0.21 W/m^2) is reported in the main text.

The estimate of one trillion tons of CO_2 emissions is computed using the following approximate formula: $f = (5.35\ W/m^2)\ \ln[x/R]$ (Myhre et al., 1998). Here f is the radiative forcing relative to an arbitrary reference value R, x is the atmospheric CO_2 concentration, and ln indicates the natural logarithm. Note that this formula is an expression of the relationship that a doubling of atmospheric CO_2 causes a radiative forcing of 3.71 W/m^2. Considering a radiative forcing of 0.71 W/m^2, this translates to an increase in the atmospheric CO_2 concentration from 400 to 456.7 ppm. Since 1 ppm of atmospheric CO_2 is equivalent to 7.77 Gt (Le Quéré et al., 2018), this increase of 56.7 ppm weighs 441 Gt. The mean airborne fraction of CO_2 (i.e., fraction of CO_2 emissions that remain in the atmosphere) is estimated to be 0.44 ± 0.06 (section 6.3.2.4 of Ciais et al., 2013). This implies that the emissions needed to increase atmospheric CO_2 enough to cause 0.71 W/m^2 of radiative forcing is 1.0 trillion tons (i.e., 441 Gt/0.44).

The CMIP5 results plotted in Figure 1 use processed model output for Arctic sea ice extent and global-mean temperature from Rosenblum and Eisenman (2017), where details of the data processing are discussed. Historical (1850–2005) and RCP4.5 (2006–2010) output from 40 CMIP5 models is analyzed. Note that the sea ice sensitivity has been shown previously to be approximately independent of the emission scenario (Rosenblum & Eisenman, 2017; Winton, 2011). The analysis in the present study uses one realization from each model (the lowest realization number available for each model). The ice extent and temperature are both annually averaged. The 1979 baseline values are computed from a linear fit to the years 1979–2016, consistent with the analysis of satellite data described above. The sea ice sensitivity is computed as the ratio between the ordinary least squares temporal linear trend in sea ice extent and global-mean temperature during years 1979–2016. In order to avoid issues associated with ice retreat saturating when it reaches zero, as well as issues associated with small numerator or denominator values in the sea ice sensitivity calculation, simulations are excluded if the ice extent falls below 1×10^6 km^2 during 1979–2016 or if the end points of the linear fits during these years do not differ by at least 0.25×10^6 km^2 of sea ice loss and 0.25°C of global warming. This led to seven of the models being excluded (model names CSIRO-Mk3-6-0, FGOALS-g2, FIO-ESM, GISS-E2-H, IPSL-CM5B-LR, MRI-CGCM3, and BCC-CSM1-1), leaving 33 models included in Figure 1. For the observations in Figure 1, we use Arctic sea ice extent from the National Snow and Ice Data Center Sea Ice Index (Fetterer et al., 2017) and global-mean temperature from the Goddard Institute for Space Sciences Surface Temperature Analysis (Hansen et al., 2010), and we analyze years 1979–2016 as in the models.

References

Acknowledgments
This study analyzes CERES satellite data, satellite sea ice concentration data, and CMIP5 model output, all of which are publicly available. This work was partially supported by IGSD (KP and IE), by a fellowship to KP from the NASA Postdoctoral Program, administered by the Universities Space Research Association, and by National Science Foundation Grant OPP-1643445 to IE.

Bender, F. A. M., Charlson, R. J., Ekman, A. M. L., & Leahy, L. V. (2011). Quantification of monthly mean regional-scale albedo of marine stratiform clouds in satellite observations and GCMs. *Journal of Applied Meteorology and Climatology*, *50*(10), 2139–2148. https://doi.org/10.1175/JAMC-D-11-049.1

Bender, F. A. M., Engstrom, A., Wood, R., & Charlson, R. J. (2017). Evaluation of hemispheric asymmetries in marine cloud radiative properties. *Journal of Climate*, *30*(11), 4131–4147. https://doi.org/10.1175/JCLI-D-16-0263.1

Cao, Y. F., Liang, S. L., Chen, X. N., & He, T. (2015). Assessment of sea ice albedo radiative forcing and feedback over the Northern Hemisphere from 1982 to 2009 using satellite and reanalysis data. *Journal of Climate*, *28*(3), 1248–1259. https://doi.org/10.1175/JCLI-D-14-00389.1

Ciais, P., Sabine, C., Bala, G., Bopp, L., Brovkin, V., Canadell, J., Chhabra, A., DeFries, R., Galloway, J., Heimann, M., Jones, C., Le Qur, C., Myneni, R. B., Piao, S., & Thornton, P. (2013). Carbon and Other Biogeochemical Cycles. In T. F. Stocker et al. (Eds.), *Climate Change 2013: The Physical Science Basis. Contribution of Working Group I to the Fifth Assessment Report of the Intergovernmental Panel on Climate Change*. Cambridge, United Kingdom and New York, NY, USA: Cambridge University Press.

Comiso, J. (2017). Bootstrap sea ice concentrations from Nimbus-7 SMMR and DMSP SSM/I-SSMIS, version 3, Natl. Snow and Ice Data Cent. Distributed Active Archive Cent, Boulder, Colo. http://nsidc.org/data/nsidc-0079.html

Eisenman, I. (2010). Geographic muting of changes in the Arctic sea ice cover. *Geophysical Research Letters*, *37*, L16501. https://doi.org/10.1029/2010GL043741

Engstrom, A., Bender, F. A. M., Charlson, R. J., & Wood, R. (2015). The nonlinear relationship between albedo and cloud fraction on near-global, monthly mean scale in observations and in the CMIP5 model ensemble. *Geophysical Research Letters*, *42*, 9571–9578. https://doi.org/10.1002/2015GL066275

Fetterer, F., Knowles, K., Meier, W., Savoie, M., & Windnagel, A. (2017). Sea ice index, version 3, Natl. Snow and Ice Data Cent, Boulder, Colo. Updated daily http://nsidc.org/data/g02135.html

Flanner, M. G., Shell, K. M., Barlage, M., Perovich, D. K., & Tschudi, M. A. (2011). Radiative forcing and albedo feedback from the Northern Hemisphere cryosphere between 1979 and 2008. *Nature Geoscience*, *4*(3), 151–155. https://doi.org/10.1038/NGEO1062

Gregory, J. M., Stott, P. A., Cresswell, D. J., Rayner, N. A., Gordon, C., & Sexton, D. M. H. (2002). Recent and future changes in Arctic sea ice simulated by the HadCM3 AOGCM. *Geophysical Research Letters*, *29*(24), 2175. https://doi.org/10.1029/2001GL014575

Hansen, J., Ruedy, R., Sato, M., & Lo, K. (2010). Global surface temperature change. *Reviews of Geophysics*, *48*, RG4004. https://doi.org/10.1029/2010RG000345

Hudson, S. R. (2011). Estimating the global radiative impact of the sea ice-albedo feedback in the Arctic. *Journal of Geophysical Research*, *116*, D16102. https://doi.org/10.1029/2011JD015804

Jahn, A. (2018). Reduced probability of ice-free summers for 1.5°C compared to 2°C warming. *Nature Climate Change*, *8*(5), 409–413. https://doi.org/10.1038/s41558-018-0127-8

Kay, J. E., & Gettelman, A. (2009). Cloud influence on and response to seasonal Arctic sea ice loss. *Journal of Geophysical Research*, *114*, D18204. https://doi.org/10.1029/2009JD011773

Kay, J. E., Holland, M. M., & Jahn, A. (2011). Inter-annual to multi-decadal Arctic sea ice extent trends in a warming world. *Geophysical Research Letters*, *38*, L15708. https://doi.org/10.1029/2011GL048008

Le Quéré, C., Andrew, R. M., Friedlingstein, P., Sitch, S., Pongratz, J., Manning, A. C., et al. (2018). Global carbon budget 2017. *Earth System Science Data*, *10*(1), 405–448. https://doi.org/10.5194/essd-10-405-2018

Millar, R. J., Fuglestvedt, J. S., Friedlingstein, P., Rogelj, J., Grubb, M. J., Matthews, H. D., et al. (2017). Emission budgets and pathways consistent with limiting warming to 1.5°C. *Nature Geoscience*, *10*(10), 741–747. https://doi.org/10.1038/NGEO3031

Morrison, A. L., Kay, J. E., Chepfer, H., Guzman, R., & Yettella, V. (2018). Isolating the liquid cloud response to recent Arctic sea ice variability using spaceborne lidar observations. *Journal of Geophysical Research: Atmospheres*, *123*, 473–490. https://doi.org/10.1002/2017JD027248

Myhre, G., Highwood, E. J., Shine, K. P., & Stordal, F. (1998). New estimates of radiative forcing due to well mixed greenhouse gases. *Geophysical Research Letters*, *25*(14), 2715–2718. https://doi.org/10.1029/98GL01908

Notz, D., & Stroeve, J. (2016). Observed Arctic sea-ice loss directly follows anthropogenic CO_2 emission. *Science*, *354*(6313), 747–750. https://doi.org/10.1126/science.aag2345

Perovich, D. (1998). Optical properties of sea ice. In M. Leppäranta (Ed.), *Physics of ice-covered seas* (Vol. 1, pp. 195–230). Helsinki: University of Helsinki.

Pistone, K., Eisenman, I., & Ramanathan, V. (2014). Observational determination of albedo decrease caused by vanishing Arctic sea ice. *Proceedings of the National Academy of Sciences of the United States of America*, *111*(9), 3322–3326. https://doi.org/10.1073/pnas.1318201111

RCP Database (2009). Historical followed by RCP8.5, Web Database. accessed Jan 30, 2018 https://tntcat.iiasa.ac.at:8743/RcpDb/dsd?Action=htmlpage&page=compare,

Rosenblum, E., & Eisenman, I. (2017). Sea ice trends in climate models only accurate in runs with biased global warming. *Journal of Climate*, *30*(16), 6265–6278. https://doi.org/10.1175/JCLI-D-16-0455.1

Screen, J. A., & Williamson, D. (2017). Ice-free Arctic at 1.5°C? *Nature Climate Change*, *7*(4), 230–231.

Sigmond, M., Fyfe, J. C., & Swart, N. C. (2018). Ice-free Arctic projections under the Paris agreement. *Nature Climate Change*, *8*(5), 404–408. https://doi.org/10.1038/s41558-018-0124-y

Wielicki, B. A., Barkstrom, B. R., Harrison, E. F., Lee, R. B., Smith, G. L., & Cooper, J. E. (1996). Clouds and the Earth's radiant energy system (CERES): An Earth observing system experiment. *Bulletin of the American Meteorological Society*, *77*(5), 853–868.

Winton, M. (2011). Do climate models underestimate the sensitivity of Northern Hemisphere sea ice cover? *Journal of Climate*, *24*(15), 3924–3934. https://doi.org/10.1175/2011JCLI4146.1

Xu, Y. Y., & Ramanathan, V. (2017). Well below 2°C: Mitigation strategies for avoiding dangerous to catastrophic climate changes. *Proceedings of the National Academy of Sciences of the United States of America*, *114*(39), 10,315–10,323. https://doi.org/10.1073/pnas.1618481114

Supporting Information for "Radiative Heating of an Ice-free Arctic Ocean"

Kristina Pistone[1]*, Ian Eisenman[2], and V. Ramanathan[2]

[1]Bay Area Environmental Research Institute, NASA Ames Research Center, Moffett Field, CA

[2]Scripps Institution of Oceanography, University of California San Diego, La Jolla, CA

Contents of this file

1. Text S1 to S2
2. Figures S1 to S6

Introduction

This file contains two sections of text and six figures. Text S1 describes updates to an earlier published analysis that is drawn on in this study. Text S2 discusses the spatial structure of albedo changes and issues related future changes in cloudiness.

Text S1 (Updates to analysis in PER2014)

The albedos and radiative forcing during 1979-2000 shown in Figure 2 are estimated using an updated version of the analysis in Pistone, Eisenman, and Ramanathan (2014, hereafter PER2014). This analysis uses the observed relationship between albedo and ice concentration in each season and region of the Arctic during the CERES period (2000-2016) to reconstruct the albedos when only sea ice observations are available (1979-2000). A more complete description of the data and methodology may be found in the Supporting Information of PER2014. The PER2014 analysis was re-run for the present study using updated CERES and sea ice concentration data through 2016. The uncertainty envelope (thin grey lines in Figure 2 of the present study) are the range of 1000 Monte Carlo simulations in which the values of the regression coefficients (two slopes and two intercepts for each region and month) are perturbed using pseudorandom numbers drawn from a normal distribution with a standard deviation equal to the 68% confidence interval for each linear regression coefficient. We use the Bootstrap sea ice concentration version 2 dataset (Comiso, 2017), which is the updated version of the dataset used in PER2014 and extends through the end of 2016 in the present analysis. PER2014 used Edition 2.6 of the CERES SSF data, which was the most current edition available at the time. Here instead we use CERES SSF data from Edition 4A, which has notable algorithm updates. These include incorporating improved snow and ice directional models as well as a change in the incorporation of twilight fluxes. Both editions are 1×1-degree monthly data. The PER2014 analysis resulted in an estimated decrease in albedo and corresponding increase in absorbed solar radiation over the Arctic Ocean for 1979 through 2011 of 4% (52% to 48%) and 6.4 ± 0.9 W/m^2, respectively. To quantify the impact of the CERES Edition updates, we note that performing an equivalent analysis with the updated CERES data for the same period as in PER2014 gives a forcing result (for 1979 through 2011) of 5.2 ± 0.9 W/m^2. Using the updated CERES data Edition for the full extended record (1979 through 2016), as in the present study, gives changes in all-sky albedo and shortwave forcing of 3.3% (51.2% to 48.0%) and 6.2 ± 1 W/m^2, respectively. A full Data Quality Summary of CERES SSF 1-degree Edition 4A, including the algorithm changes from previous Editions, may be found at https://ceres.larc.nasa.gov/documents/DQ_summaries/CERES_SSF1deg_Ed4A_DQS.pdf

Text S2 (Discussion of albedo and cloud conditions)

We consider locations to be ice-free in this analysis if the sea ice concentration is zero. For this we use the 1×1-degree monthly gridded snow/ice percent field reported with the CERES data product, which is derived from passive microwave measurements. Although there are many factors which can contribute to changes in planetary albedo, including atmospheric aerosol concentrations, water vapor, surface type, and sea ice concentration and properties, we find that the dominant factor governing clear-sky planetary albedo above ice-free locations in the Arctic Ocean is the solar zenith angle (SZA), which is governed by both the cosine of latitude and the season based on orbital geometry. Thus, in the simplest case of a cloud-free, ice-free open ocean, the observed Arctic albedo is found to be primarily a function of the SZA alone (Figure S1) (note that other factors are clearly present and may help explain outliers, including notable wildfire conditions in April 2007 which produced anomalously high albedos over the open ocean). Here, SZA is calculated in each grid box for solar noon, mid-month conditions. The monthly average albedo values included with the CERES SSF data for each grid box are used. The fit of the clear-sky albedo vs SZA relationship for all months combined (black dashed line in Figure S1) is adopted here to estimate the seasonally-varying clear-sky albedo field for an ice-free Arctic Ocean based on the SZA of each grid box in each month.

As discussed in the main text, accounting for the effects of clouds on the planetary albedo results in a more complicated picture. Previous work has established a straightforward linear dependence of scene albedo on cloud fraction (Bender,

*kristina.pistone@fulbrightmail.org

0094-8276/19/$5.00

Charlson, Ekman, & Leahy, 2011) for a uniform cloud population. However, when variability in cloud conditions (including fraction [f_{cld})], type, and optical thickness [τ_{cld}]) and viewing geometry (including varying SZA) are included, the observed albedos instead exhibit a markedly nonlinear relationship which depends on the properties of the clouds considered. Previous studies have noted similar results (Bender, Engstrom, Wood, & Charlson, 2017; Engstrom, Bender, Charlson, & Wood, 2015). We account for this by considering individual populations of fully overcast conditions (defined as $f_{cld} > 95\%$) for defined ranges of cloud optical depths (Figure S2). This allows us to calculate an overcast albedo for each binned range of SZA and τ_{cld}. From these, a baseline estimate overcast albedo is calculated by weighting each grid box according to the observed frequency distribution of cloud optical depths (Figure S3) for all ocean conditions (ice-free as well as ice-covered). An example of the spatial distribution of cloud fraction is given in Figure S4, with the corresponding estimate of average-cloudiness albedo. The seasonal cycles of overcast albedo for a given cloud optical depth (Figure S5, colored lines) and for an average overcast condition when weighted by the cloud optical depth incidence (Figure S5, grey line) are also shown.

Finally, the baseline estimate all-sky albedo is calculated from the clear-sky and average overcast albedos using the dependence of the latter on cloud fraction (Bender et al., 2011) for each gridded (lat,lon) point, where the clear-sky and overcast values are weighted according to the 17-year observed mean cloud fractions at each location under all ocean surface conditions. The assumption that an ice-covered location will retain the same average cloud properties (τ_{cld}, f_{cld}) if instead it becomes ice-free is a limitation of the current study, due to the lack of observations of ice-free midsummer conditions in some Arctic Ocean regions. However, as discussed in the main text, this may be a relatively accurate approximation for ice loss during midsummer (Morrison, Kay, Chepfer, Guzman, & Yettella, 2018), which is the period with greatest insolation. Indeed, the range of albedos corresponding to different cloud optical depth assumptions (Figure S5) as they relate to the weighted-average overcast albedos, particularly when combined with the distributions of observed cloud optical depths (Figure S3), offers an additional perspective on the range of potential ice-free albedos in the case of potentially changing cloud properties.

From the estimate described above, the spatial average of ice-free, average-cloudiness albedo is then weighted according to the ocean surface area and monthly-averaged insolation to arrive at the values reported in the text. Intermediate steps are also plotted below: ice-free all-sky albedo by month (Figure S5, black line) and by latitude (Figure S6).

References

Bender, F. A. M., Charlson, R. J., Ekman, A. M. L., & Leahy, L. V. (2011). Quantification of monthly mean regional-scale albedo of marine stratiform clouds in satellite observations and GCMs. *J. Appl. Meteorol. Climatology*, *50*(10), 2139–2148. doi: 10.1175/JAMC-D-11-049.1

Bender, F. A. M., Engstrom, A., Wood, R., & Charlson, R. J. (2017). Evaluation of hemispheric asymmetries in marine cloud radiative properties. *J. Climate*, *30*(11), 4131–4147. doi: 10.1175/JCLI-D-16-0263.1

Comiso, J. (2017). Bootstrap sea ice concentrations from Nimbus-7 SMMR and DMSP SSM/I-SSMIS, version 3. *Natl. Snow and Ice Data Cent. Distributed Active Archive Cent., Boulder, Colo.*. (http://nsidc.org/data/nsidc-0079.html)

Engstrom, A., Bender, F. A. M., Charlson, R. J., & Wood, R. (2015). The nonlinear relationship between albedo and cloud fraction on near-global, monthly mean scale in observations and in the CMIP5 model ensemble. *Geophys. Res. Lett.*, *42*(21), 9571–9578. doi: 10.1002/2015GL066275

Morrison, A. L., Kay, J. E., Chepfer, H., Guzman, R., & Yettella, V. (2018). Isolating the liquid cloud response to recent Arctic sea ice variability using spaceborne lidar observations. *J. Geophys. Res.-Atmospheres*, *123*(1), 473–490. doi: 10.1002/2017JD027248

Pistone, K., Eisenman, I., & Ramanathan, V. (2014). Observational determination of albedo decrease caused by vanishing Arctic sea ice. *Proc. National Acad. Sciences United States Am.*, *111*(9), 3322–3326. doi: 10.1073/pnas.1318201111

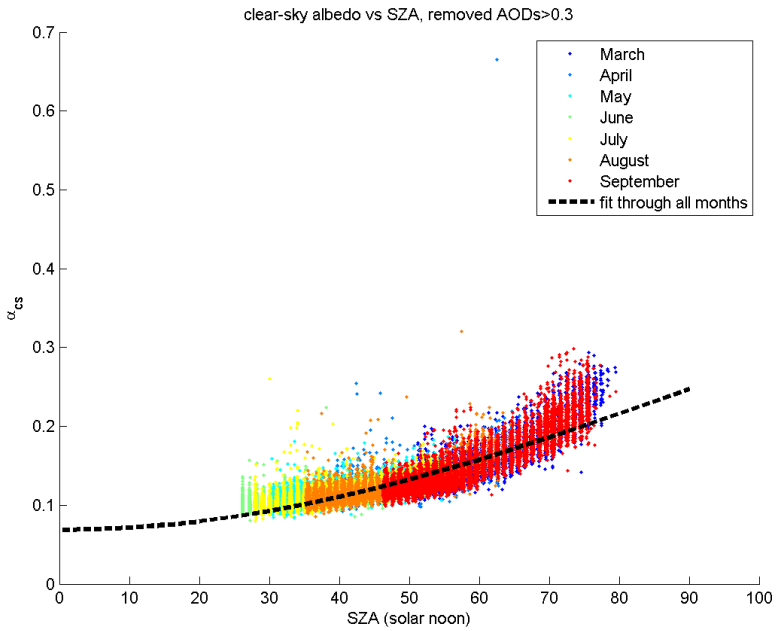

Figure S1. Observed CERES monthly-averaged clear-sky ice-free albedo (α_{cs}) as a function of solar zenith angle (SZA), for the years considered (2000-2016), colored by month. Here each plotted point represents an ice-free Arctic Ocean grid box in the CERES data. The relationship between SZA and α_{cs} can be seen to be approximately constant across all months, despite the variation in latitude. Note from this figure that the assumption of a linear fit to the cosine of SZA may result in an underestimation of α_{cs} at very high SZA and an overestimation of α_{cs} at midrange values of SZA.

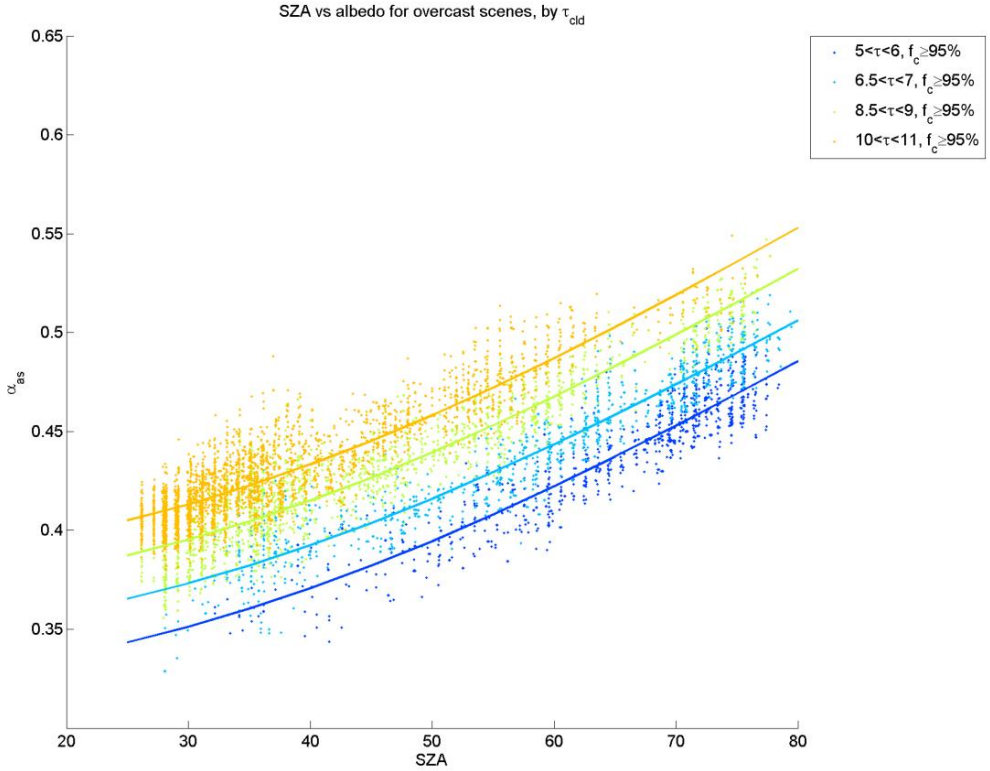

Figure S2. Linear fits of overcast albedo to the cosine of SZA for different cloud optical depth populations. Note that only a subset of the cloud populations used in the full analysis is plotted here in order to highlight the correlation within a given population. The full range of cloud optical depth (τ_{cld}) bins are shown in Figure S5.

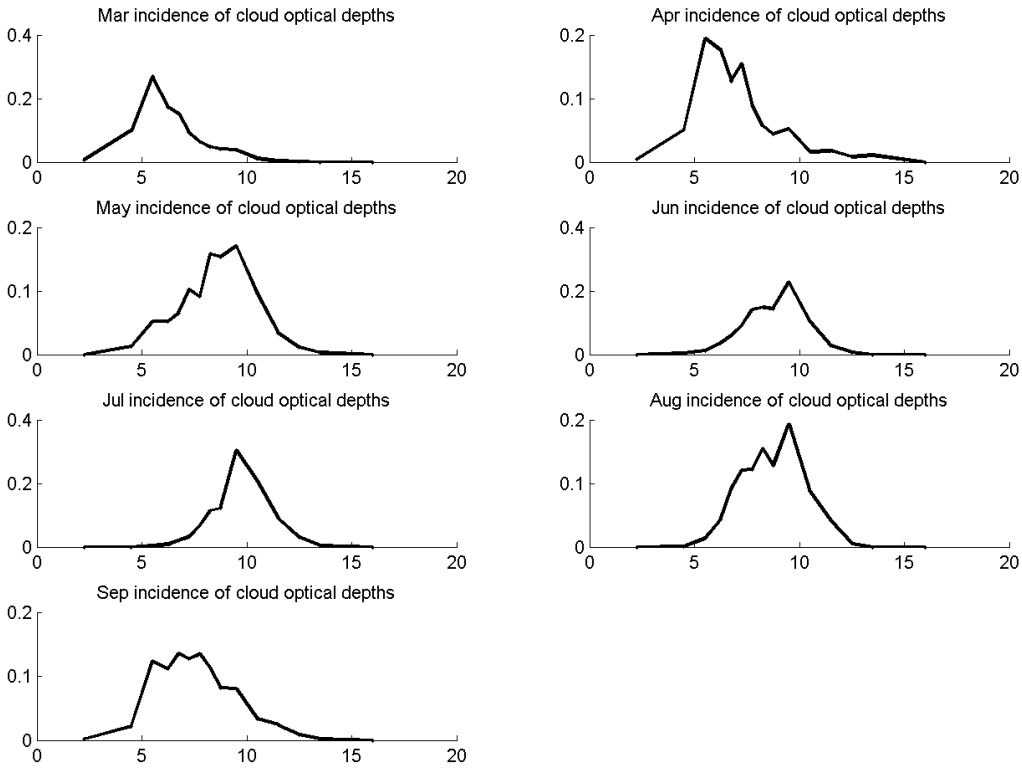

Figure S3. Cloud optical depth frequency by month under all ocean conditions.

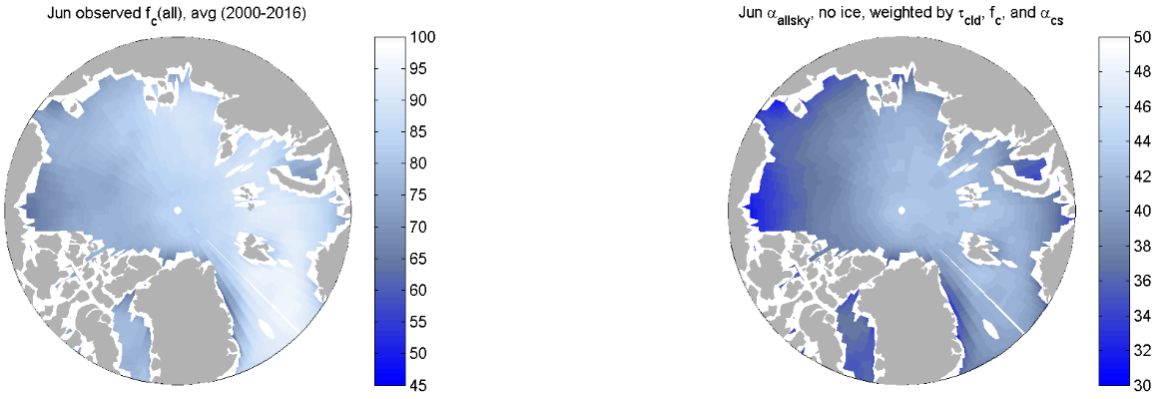

Figure S4. An example of (left) the average cloud fraction above the Arctic Ocean used in the cloud condition estimate, and (right) the resulting spatial distribution of average cloud optical depth.

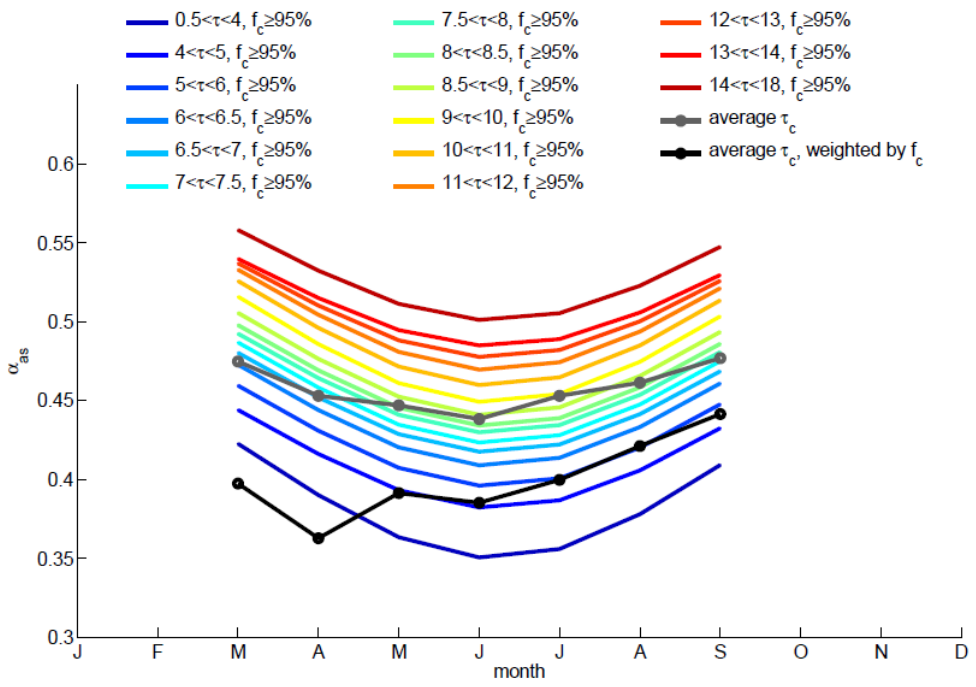

Figure S5. Monthly overcast albedo under different cloud optical depths (colored lines), monthly overcast albedo corresponding to the average cloud optical depth (grey line), and monthly all-sky albedo computed by weighting the average overcast albedo by the cloud fraction (black line).

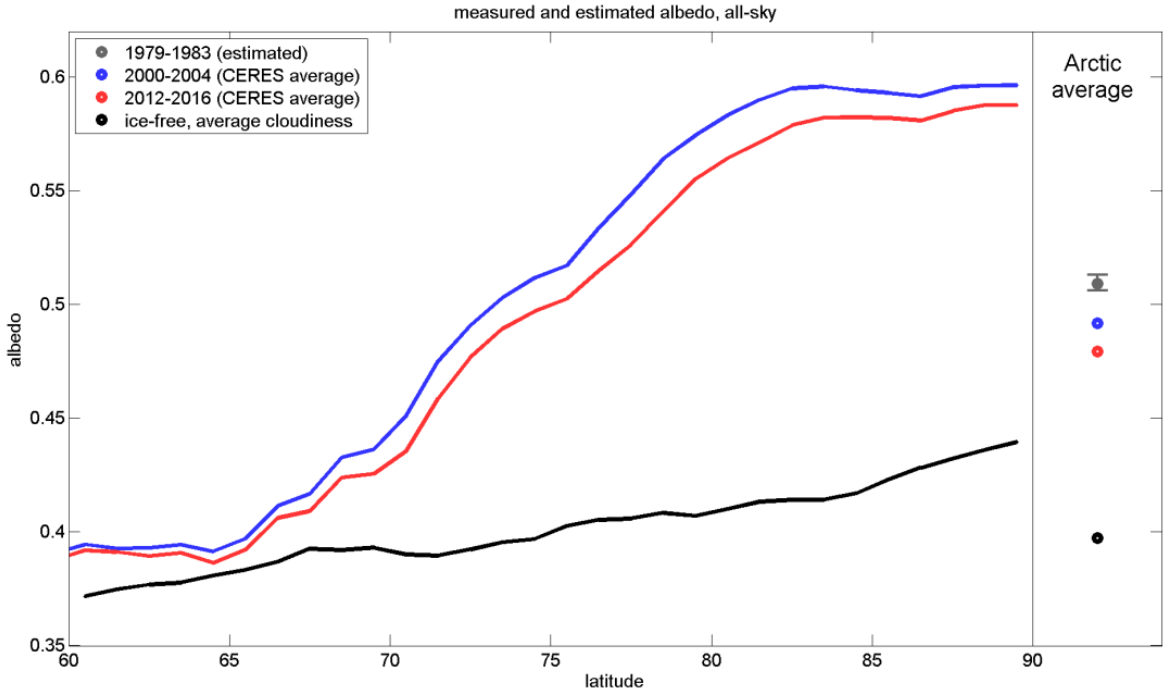

Figure S6. All-sky albedo as a function of latitude for 5-year averages during the observational period and for the estimated change under a transition to ice-free conditions from a 1979 baseline state. The average value over the Arctic Ocean during 1979-1983 is shown as a grey circle on the right side of the figure, with Arctic Ocean spatial averages associated with the 3 curves also included for reference.